2026 IEEE International Conference on Robotics and Automation (ICRA 2026)
June 1-5, 2026. Vienna, Austria

# A Path Planning Strategy for Robotic Bronchoscopic Multi-sample Biopsy

Qiqi Pan[1], Jingjing Luo[1], Yongfei Feng[1,2], Wenke Duan[3], Shijie Guo[1], Hongbo Wang[1,*], *Member, IEEE*

***Abstract*— Lung cancer is the leading cause of cancer death globally, and early diagnosis via transbronchial biopsy (TBB) improves outcomes. However, conventional bronchoscopes for multiple pulmonary nodules face inefficiencies and operator skill dependency. This paper proposes a path planning strategy for robotic bronchoscopic multi-sample TBB. It abstracts the bronchial tree as a circuit, with lesions as constant-resistance bulbs and bronchial branches as resistors with equivalent resistance based on their morphology. Multi-target path planning is transformed into minimizing total circuit resistance, optimizing trajectories to reduce redundant movements of robotic manipulators. Comparing to traditional methods, evaluations show that over 60% reduced movement distance and 76% less operation time are achieved; experiments accomplish over 40% efficiency improvement, enhancing multi-sample TBB efficiency and safety.**

## I. Introduction

Lung cancer is the most common cause of cancer death worldwide, but early diagnosis can significantly increase the cure and survival rate, and improve the quality of prognosis of patients [1]. Common diagnostic and treatment methods include computed tomography (CT) screening, Percutaneous lung biopsy [2], bronchoscopic biopsy [3], etc. Although CT screening can improve the biopsy success rate of early lung cancer, there is a certain false positive rate and risk of overdiagnosis [4]. Percutaneous biopsy may cause pulmonary bleeding and may have the risk of damaging lung tissue.

As a critical approach for the early screening of pulmonary nodules, transbronchial biopsy (TBB) offers distinct advantages of high diagnostic accuracy, low complication incidence, and minimal invasiveness [5]. Nevertheless, the application of conventional bronchoscopes in TBB is hindered by issues such as inadequate lesion localization and significant operator skill dependency. The utilization of flexible bronchoscopic robotic systems for TBB can effectively improve diagnostic yield and procedural safety profiles. The pulmonary bronchial tree exhibits a hierarchical multi-level structure, with a high degree of anatomical similarity among bronchi at each hierarchical level. This inherent characteristic renders it challenging to achieve target localization using solely CT scans or endoscopic images. Thus, the establishment of a robust bronchial navigation strategy and the formulation of a bronchoscopic robot's motion trajectory represent critical prerequisites for successful TBB procedures. Clinically, multiple small pulmonary nodules are a prevalent scenario, necessitating the investigation of optimal multi-target path planning methods that can identify the optimal trajectory under specified constraints—thereby ensuring efficient lesion detection and intervention.

Bronchial navigation tasks based on traditional path planning algorithms have been widely studied to assist the positioning and movement of endoscopes for TBB [6]. However, most existing studies rely on traditional path planning algorithms, which only consider the actual movement distance from the initial point to the target point and obstacle constraints, and do not consider the impact of the actual structure (curvature, cavity diameter, etc.) inside the bronchial cavity on the movement of the endoscope. In addition, existing studies generally only consider the path planning problem of a single target point in the bronchus, which is more effective for some lesions with clear locations and close to the natural channels of the bronchus, such as central lesions or lung lesions close to the bronchi [7]. However, existing studies cannot effectively and efficiently solve the problem of multi-target point path planning and navigation optimization for the symptoms of multiple pulmonary nodules.

The optimization of bronchoscopic robot navigation tasks typically begins with a skeletonization algorithm [8] to extract the centerline of the bronchial structure, which serves as the initial path for planning task. Different from general obstacle avoidance planning tasks, the working environment of a bronchoscopic robot is confined to narrow spaces of the bronchi. Its navigation task can be abstracted as identifying the optimal path from a fixed set of multiple paths.

Existing bronchoscopic path planning strategies are predominantly rooted in classic algorithms, including Euclidean coordinate search [9], "reverse planning, forward navigation" [10], reverse planning framework with rapidly exploring random tree (RRT) [11], etc. Besides, some other studies focus on visual-based navigation [12], [13], estimating bronchoscope position or enabling real-time tracking. For multi-target path planning problems, domain knowledge-based genetic algorithm (DKBGAMT) [14], heuristic algorithm based on RRT [15], RGHG-RRTs algorithm [16] are proposed to achieve multiple target. In addition, a needle path planning method based on Bee Foraging Learning Particle Swarm Optimization algorithm (BFL-PSO) [17] and a multi-target path planning algorithm with target sorting and partial retraction [18] are developed in surgical scenarios, offering feasible and referable solutions for TBB path planning.

Inevitably, existing methods applied to bronchoscopes are

*This research was funded by National Key R&D Program of China under Grant 2024YFF1206900.

[1]The authors are with College of Intelligent Robotics and Advanced Manufacturing, Fudan University, Shanghai, China.

[2]The author is with Faculty of Mechanical Engineering and Mechanics, Ningbo University, Zhejiang, China.

[3]The author is with Shenzhen Institutes of Advanced Technology, Chinese Academy of Sciences, Guangdong, China.

*Corresponding author (e-mail: wanghongbo@fudan.edu.cn).

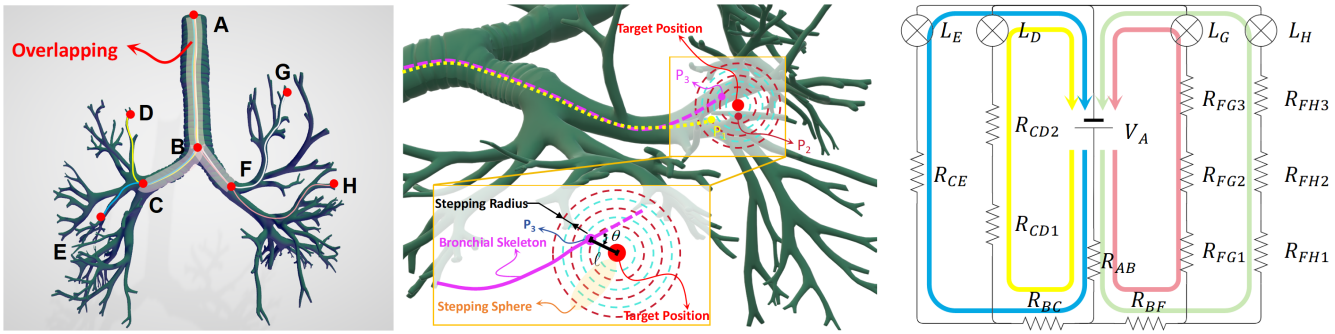


(a) (b) (c)

Fig. 1. Equivalent circuit of the bronchial model. (a) Overlapping paths of bronchoscope during multi-sample TBB operation. (b) Three suitable biopsy points for a specified lesion. (c) Equivalent circuit of the bronchoscopic pathway.

oriented toward a single TBB target, failing to address how to improve the efficiency in the presence of multiple pulmonary lesions. Existing multi-target planning methods did not account for the multiple positional possibilities of a single target or the combined optimal solution for multiple variable targets, thus failing to find the solution.

This paper presents an optimized planning strategy for determining optimal path to multiple targets. The multi-lesion inspection task of bronchoscope is abstracted as a problem of finding the loop path with minimal resistance within an electrical circuit loop (this strategy is also applicable to single-target path planning).The main contributions of this paper are as follows:

1) This strategy simplifies the multi-lesion biopsy task in bronchus into an equivalent circuit problem for solving the minimum resistance value by integrating the similar characteristics between bronchial branches and circuit branches.

2) The impacts of bronchial morphology, lesion locations, etc., on TBB are simplified into weighted resistances in the circuit, enabling dimensionality-reduction analysis.

3) The proposed method enables automatic solution of TBB routes (both for single and multiple inspections in one session), and can be implemented in conventional bronchoscopes or bronchoscopic robots, significantly enhancing the efficiency of biopsying multiple pulmonary nodules.

## II. Methodology

This research aims to propose a method for identifying the optimal path, which can be explicated as follows: A hypothetical line connects the bronchial lesion (to be examined) and the main bronchial orifice, with the lesion modeled as a bulb (with constant resistance) in an electrical circuit. Current is released from the main bronchus, flowing through the bronchial tree toward the bulb, which lights up upon current passage. The optimal path is defined by the current trajectory that maximizes the bulb's brightness. For the problem of multiple pulmonary nodules, the number of bulbs to be lit similar to the above situation increases, and multiple paths will overlap, as shown in Fig. 1a.

In order to improve the efficiency of TBB, the overlapping path should be designed to be passed no more than twice (including retraction) when the bronchoscopic manipulator is operated. For example, when there are four target points D, E, G, and H in the bronchus shown in Fig. 1a, when the four optimal paths are found respectively, the four paths overlap in the AB segment, the paths to the two target points D and E overlap in the BC segment, and the paths to G and H overlap in the BF segment. When doing one-sample TBB operation, the moving path of bronchoscopic manipulator is A→B→C→D→C→B→A→B→C→E→C→B→A→B→F→G→F→B→A→B→F→H; when applying multi-sample TBB operation, the path simplifies to A→B→C→D→C→E→C→B→F→G→F→H. It is evident that for multiple pulmonary nodules, the multi-sample TBB significantly enhances detection efficiency and operational convenience. This paper aims to identify the most efficient and operationally convenient pathway for bronchoscopic robots to perform multi-target biopsies in a single bronchial insertion.

### A. Selection of the Target Positions

According to different lesion locations of TBB, lesions can be divided into lesions within the trachea and bronchial cavity, diffuse pulmonary lesions, focal pulmonary lesions, extrabronchial lesions, peripheral lung lesions, etc. [19]. For lesions inside the bronchus, the bronchoscopic robot can directly obtain the optimal path from the initial end of the trachea to the target point of the lesion using an appropriate path planning algorithm; for lesions outside the bronchus, the bronchoscopic robot may have multiple feasible paths from the initial end of the trachea to the target point.

To reduce classification complexity, for endobronchial lesions, biopsy forceps can typically be used for direct sampling, so the equivalent resistance at the lesion site is defined as a constant value $\eta$. For extrabronchial lesions, transbronchial needle aspiration (TBNA) is generally required, and the equivalent resistance at the lesion site is affected by factors such as the distance from the lesion to the bronchus and the needle insertion angle. Thus, the equivalent resistance is determined as follows: taking the position of the lesion site as a sphere center, the spherical radius is gradually expanded (with a step $s_t$ of 0.2 mm), and the upper limit of the radius is set to 40 mm (not exceeding the maximum

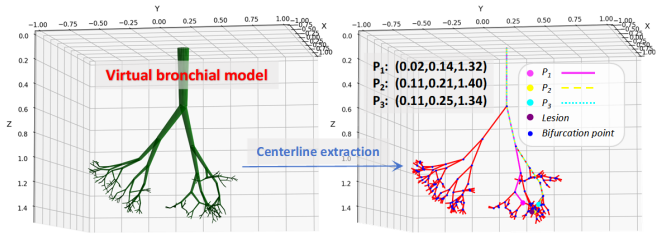


Fig. 2. Selection of three feasible biopsy sites when the lesion is located outside the bronchus.

needle insertion length of commonly used biopsy needles [20]). $P_1$ is the intersection point with the smallest $\theta$ (see Fig. 1b), which is the angle between the bronchial centerline and the connecting line between the spherical surface and the target point; $P_2$ is the point where the spherical surface first contacts the centerline during the process of gradually expanding the sphere, that is, the point with the minimum $\ell$ (see Fig. 1b), which represents the Euclidean distance from $P_2$ to the location of the lesion; $P_3$ is the point with the maximum value of a weighted function $\varphi$ of $\ell$ and $\theta$, i.e., the point with $\max_{\ell,\theta} \varphi(\ell, \theta)$. $\varphi$ is defined as

$$\varphi = W_\ell \cdot \ell + W_\theta \cdot \theta \tag{1}$$

where $W_\ell$ and $W_\theta$ respectively represent the weight coefficients of the two parameters, which are determined by (2):

$$W_\theta = \frac{k \cdot \frac{L}{S}}{1 + k \cdot \frac{L}{S}} \cdot W_\ell = 1 - W_\theta \tag{2}$$

where $S$ and $L$ represent the diameter and the biopsy depth of the lesion, respectively. $k$ is the calibration coefficient, usually taken as 0.5-2.

The three points $P_1$, $P_2$, $P_3$ obtained by the process above are used as the target points of extrabronchial lesions, and the subsequent path planning and equivalent resistance calculation are carried out on this basis. When the lesion is located outside the bronchus, the three corresponding internal positions can be found as Fig. 2 shows. For the three target points found, the DFS method can be used to plan the routes, which are marked in different colors in Fig. 2.

### B. Definition of Equivalent Resistance

Considering that bronchial bifurcation and bronchial hierarchy affect the difficulty of bronchoscope insertion, the concept of "Equivalent Resistance" for bronchial branches at each level is introduced. The dimensionless equivalent resistance of $i$-th order bronchus is defined as $Z_i$, which can be expressed as:

$$Z_i = \alpha \cdot \frac{L_i}{D_i} + \beta \cdot C_i + \gamma \cdot B_i \tag{3}$$

where $L_i$, $D_i$ and $C_i$ represents the length, the average diameter and the complexity (i.e., the angle with its preceding order bronchus) of the $i$-th order bronchus, respectively. $B_i$ represents other physical characteristics of the $i$-th order bronchus (in this research, when there is a cartilage ring, $B_i = 1.0$; when there is no cartilage ring, $B_i = 0$). $\alpha$, $\beta$, $\gamma$ respectively represent the weight coefficients of each factor, which were set to 1.0, 0.2, and 0.5 (by manual parameter tuning).

When multi-sample TBB is performed, in order to improve the efficiency, the bronchoscopic manipulator should repeatedly pass through some bronchi, which are defined as the "overlapping paths" (refer to Section II-C), which affects the subsequent calculation of equivalent resistance. For an $i$-th order bronchus (left side of the lung), its equivalent resistance can be expressed as $[Z_i, label_{position}, label_i]$, where $label_{position}$ indicates the left side (= 1) or right side (= 2) of the lung where the bronchus is located, and $label_i$ indicates the bronchial order. For example, for the BC segment bronchus in Fig. 1a, assuming that its length is 40 mm, its average diameter is 10 mm, its angle with the preceding bronchus is $\pi/3$, and it has cartilage rings, its resistance $Z_{BC}$ can be calculated as 7.12 according to (3). According to Fig. 1a, the final equivalent resistance of this segment of bronchus can be expressed as $[7.12, 1, 1]$.

### C. Definition of the Circuit-Inspired Method

A "circuit-inspired method" is proposed for multi-sample TBB path planning. Multiple lesions are considered analogous to constant-resistance light bulbs, while the resistances from the tracheal origin to the lesions—including branch resistances and lesion-induced resistances—are treated as circuit resistors, and the movement of bronchoscopic manipulator from tracheal origin to lesions is modeled as the flow of electric current from a power source through light bulbs to illuminate them.

Assuming the four paths in Fig. 1a are the planned optimal routes, the multi-target path planning can be analogized to a circuit with bulbs, as shown in Fig. 1c. In Fig. 1c, $R_x$ denotes the resistance of bronchial segment $x$; $L_y$ represents the light bulb corresponding to leison $y$; $V_A$ signifies the power supply abstracted from the tracheal origin at point $A$.

As can be seen from Fig. 1c, all of the four loops flow through the resistor $R_{AB}$; the yellow and blue loop current paths both pass through the resistor $R_{BC}$; the red and green loop current paths both pass through the resistor $R_{BF}$.

Assume there are $N_L$ and $N_R$ lesions (bulbs) in the left and right lobes, respectively. Multiple different equivalent circuits are derived using steps described in Section II-D. The resistance of each equivalent circuit is calculated as follows, also shown in Fig.3a (resistors are ordered from closest to farthest from the power source):

1. Sum all **bronchial resistances** and **lesion resistances** of non-overlapping segments in each circuit branch. Divide the bronchi into left and right sides based on pulmonary bronchial anatomy, then compute the equivalent resistances of all bronchial orders for each path using the method in Section II-B. Calculate the resistance values across all circuits and count the number of loops each resistor is in.

2. When there is only one loop a certain resistor is in, this resistor should be connected in series with the corresponding

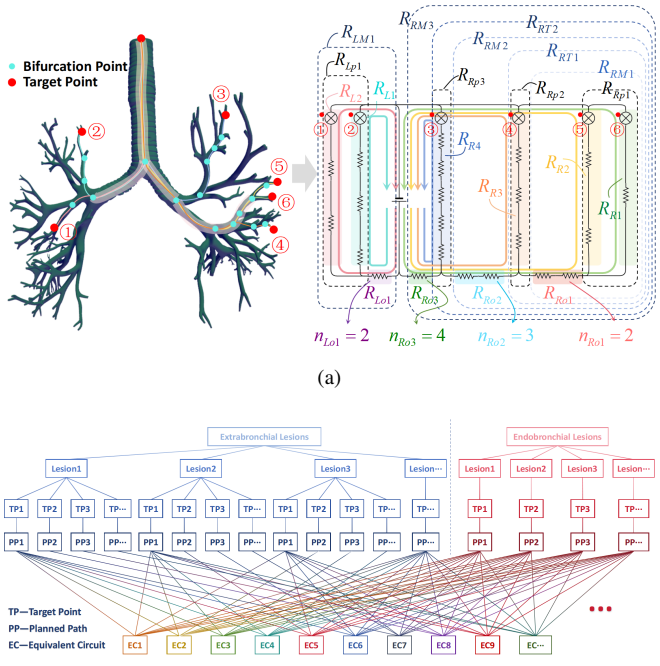


Fig. 3. Steps of obtaining the equivalent circuit. (a) Calculating the equivalent resistance of the equivalent circuit. (b) Combination of different PPs from lesions for multi-sample TBB.

bulb, then calculate the resistances as $R_{L1}, R_{L2}, \cdots$ (subscript $L$ for left) and $R_{R1}, R_{R2}, \cdots$ (subscript $R$ for right). The other resistors with the same number of loops ($\geq 2$) they are in, i.e., with the same $n_{Loi}$ or $n_{Roi}$ ($i = 1, 2, 3 \cdots$), are connected in series to calculate the corresponding $R_{Loi}$ and $R_{Roi}$ and are arranged in ascending order of $n_{Loi}$ and $n_{Roi}$ respectively.

3. Traverse all branches where the bulbs are located. If the preceding branch are the same, calculate the equivalent parallel resistance $R_{Lpi}$ ($R_{Rpi}$), and arrange them in ascending order of the preceding $n_{Loi}$ ($n_{Roi}$) as $R_{Lp1/Rp1}, R_{Lp2/Rp2}, \cdots$.

4. According to the arranged order of $R_{Lo}$ ($R_{Ro}$) and $R_{Lp}$ ($R_{Rp}$), the first $R_{Lo1}$ ($R_{Ro1}$) and $R_{Lp1}$ ($R_{Rp1}$) are connected in series to calculate the equivalent resistance $R_{LM1}$ ($R_{RM1}$). $R_{LM1}$ ($R_{RM1}$) is then connected in parallel with the preceding $R_{Lp2}$ ($R_{Rp2}$) as $R_{LT1}$ ($R_{RT1}$), and then connected in series with the preceding $R_{Lo2}$ ($R_{Ro2}$) to calculate the equivalent resistance $R_{LM2}$. The rest may be deduced by analogy.

5. Connect the last calculated $R_{LM}$ and $R_{RM}$ in parallel to calculate the resistance $R$ of the entire circuit.

The key to obtaining the equivalent circuit and equivalent resistance is to find the bifurcation point and the number of overlaps of the branches. The implementation code framework can refer to algorithm 1.

### D. "Minimum Resistance" Path Planning Strategy

The main code framework can be found in algorithm 2.

In order to implement the aforementioned steps and find the optimal circuit with the minimum equivalent resistance,

**Algorithm 1** Calculate Equivalent Resistances

**Input:** All planned paths (PPs)
Initialize: $R_{Lo/Ro}, R_{Lp/Rp}, R_{LM/RM}, R_{LT/RT} \leftarrow \emptyset$
**for** side $\in$ {left, right} **do**
  $branches \leftarrow$ Extract all branches in *side* from PPs
  **for** each branch in $branches$ **do**
    $R_{branch} \leftarrow$ Sum of bronchial resistances & lesion resistances
    $eq\_resistances[side] \leftarrow$ Compute equivalent resistances for all bronchial orders
  **end for**
  $loop\_counts[side] \leftarrow$ Count loop occurrences for each resistor in $eq\_resistances[side]$
  **for** each resistor $r$ in $eq\_resistances[side]$ **do**
    **if** $loop\_counts[side][r] == 1$ **then**
      Add series resistance of $r$ and $\eta$ to $R_{side}$
    **else**
      Group resistors / compute series resistances
      Add to $R_{Lo}$ or $R_{Ro}$ and sort by loop count
    **end if**
  **end for**
  **for** each branch with identical preceding branch **do**
    Compute parallel resistance, adding to $R_{Lp}$ / $R_{Rp}$
  **end for**
  Sort $R_{Lp}$/$R_{Rp}$ by preceding loop counts
  **for** $i \leftarrow 1$ to max(length($R_{Lo/Ro}$, $R_{Lp/Rp}$) **do**
    $R_{LM/RM}[i] \leftarrow$ Series($R_{Lp/Rp}[i]$, $R_{Lo/Ro}[i]$)
    $R_{LT/RT}[i] \leftarrow$ Parallel($R_{LM/RM}[i]$, $R_{Lp/Rp}[i]$)
  **end for**
**end for**
$R \leftarrow$ Parallel($R_{LM}$, $R_{RM}$)
**Output:** $R$

it is necessary to place the biopsy target point (bulb) and the bronchi (resistors) at appropriate positions in the circuit. As can be seen from Fig. 3b, the number of target points determines the number of branches in the equivalent circuit, and the number of bronchial bifurcations that the path passes through determines the number of resistors on the equivalent circuit. Therefore, the "minimum resistance" path planning strategy can be mainly divided into the following steps:

1. Construct a 3D model of the bronchus using CT sequence images and extract its centerline.

2. Find the lesion location in the 3D model, and calculate the equivalent resistance according to Section II-A (lesions outside the bronchus may have multiple feasible target points, resulting in multiple equivalent resistances).

3. All target points generated by the lesions are arranged and combined to generate equivalent circuits. Only one target point is taken from each lesion for planning each time. The planning method adopts the Depth First Search (DFS) algorithm [21]. The specific selection and arrangement and combination of all planned paths are shown in Fig. 3b.

4. The process from the planned path (PP) to the equivalent circuit (EC) in Fig. 3b requires determining the resistance of

**Algorithm 2** Main Procedure for multi-sample TBB Path Planning

$CT\_images \leftarrow$ load_CT_images()
$bronch\_model \leftarrow$ BUILD_3D_MODEL($CT\_images$)
$centerline \leftarrow$ EXTRACT_CENTERLINE($bronch\_model$)
$lesions \leftarrow$ DETECT_LESIONS($bronch\_model$)
$lesion\_targets \leftarrow \emptyset$
**for** each $lesion$ in $lesions$ **do**
    $targets \leftarrow$ GENERATE_TARGETS($lesion$)
    $resistances \leftarrow$ CALC_EQUIV_RES($targets$)
    $lesion\_targets.append((targets, resistances))$
**end for**
$all\_circuits \leftarrow \emptyset$
DFS_COMBINATIONS($lesion\_targets, 0, [], all\_circuits$)
**for** each $circuit$ in $all\_circuits$ **do**
    SETUP_CIRCUIT($circuit$) ▷ Resistor values
    COMPUTE_TOTAL_R($circuit$)
**end for**
$optimal\_circuit \leftarrow \arg\min_{c \in all\_circuits} c.total\_R$
**return** $optimal\_circuit$

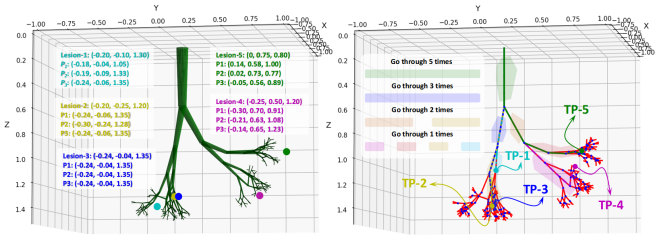


Fig. 4. The number of times each bronchus segment is passed under the path corresponding to the minimum equivalent resistance value.

each equivalent resistor and the circuit branch in which it is located, specifically following the steps in Section II-C.

5. Compare $R$ of all ECs (Fig. 3b) and select the EC with the minimum $R$. This EC is the optimal path of TBB.

In order to make the process of calculating the equivalent resistance more intuitive and simple, the equivalent resistance under each EC is calculated in the order of: terminal bronchus → primary bronchus in the form of parallel + series merging layer by layer until there are no more merging items.

## III. Evaluation

### A. Virtual Bronchial Model Simulation

Although existing software or open-source algorithms can facilitate constructing bronchial structures and extracting the centerlines, this process necessitates detailed manual intervention and model corrections [22]–[25]. To avoid extensive manual reconstruction and enable simulation validation across as many distinct bronchial models as possible, it is critical to rapidly generate a large volume of bronchial models for use as data samples.

In general, as the number of bronchial branches increases, the branching angle gradually increases, from about 21° at the 5th order to about 50° at the 15th order, and the

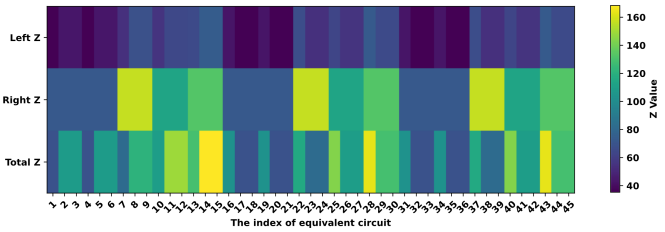


Fig. 5. Equivalent resistance distribution of different ECs based on the five lesion locations in Fig. 4.

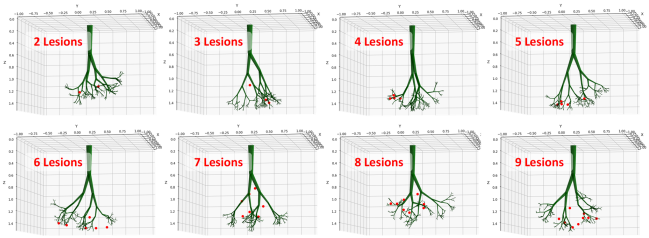


Fig. 6. Schematic diagram of different numbers of lesions specified in different bronchial models.

anterior branch angle is usually smaller than the posterior branch angle [26]. Based on this basis and some other existing methods [27], [28], 100 random morphological 8-order bronchial models were established. Then, the centerline of the bronchus was extracted, all bifurcations were marked with blue dots, as the example in Fig. 2 shows.

As shown in Fig. 4, there are 5 lesions (4 extrabronchial lesions and 1 endobronchial lesion) in the bronchial model. According to Fig. 3b, ECs are obtained, and all duplicates with the same results are removed, and there are a total of 45 final ECs. Assume that $\eta = 1.0$, the resistance value $Z$ distribution of different ECs is shown in Fig. 5.

The final selected EC with the minimum equivalent resistance is shown in Fig. 4, which marks the number of times the bronchoscope has passed through each segmented path in different color blocks.

If the number of multiple nodules in the lungs exceeds 10 and is diffusely distributed, it is usually more likely to be caused by extrathoracic malignant tumor metastasis or active infection, and the possibility of primary lung cancer is relatively small. Therefore, the number of lesions is set to 3 - 9 (the lesion position is randomly generated within the lung space, and the generated lesion coordinates are used as the basis for subsequent planning) for 100 8-level bronchial models. The planning time of these virtual models are tested for each number of lesions. The example diagrams of different numbers of lesions in different bronchial models are shown in Fig. 6. The process was performed on a PC equipped with an Intel i9-14900HX CPU, 32 GB RAM, and a single Nvidia RTX 4070 GPU with 8 G VRAM.

Assuming that the speed of the bronchoscope remains consistent, Fig. 7 records the average planning time reduction percentage (compared with traditional one-sample TBB) of 3-9 lesions under the same bronchial model. As can be seen from Fig. 7, multi-sample TBB was reduced in time by an

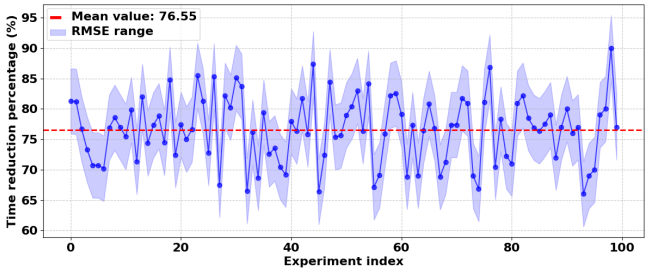


Fig. 7. Compared with the traditional one-sample TBB, the time reduction percentage of the multi-sample TBB method.

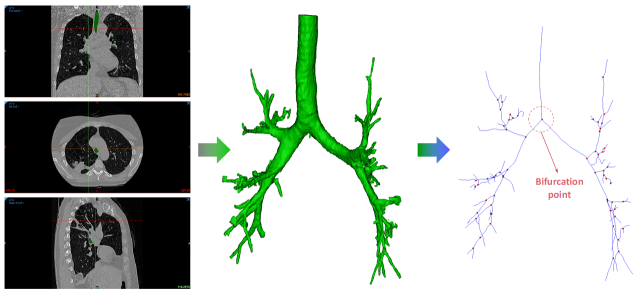


Fig. 8. Bronchial 3D reconstruction and centerline extraction process based on human CT sequence images.

average of more than 76% compared to one-sample TBB.

In order to illustrate the stability of the proposed method compared with the traditional method, the Root Mean Square Error (RMSE) of all data in Fig. 7 is calculated using (4):

$$RMSE = \sqrt{\frac{1}{n}\sum_{i=0}^{n-1}\left(t_i - \hat{t}\right)^2} \tag{4}$$

where $t_i$ represents the data value with experiment index $i$, $\hat{t}$ represents the mean of all data, and $n$ represents the total number of all indexes. The RMSE of all data in Fig. 7 is 5.37%, indicating that the data dispersion is low and the overall distribution is relatively concentrated. This shows that the proposed method can stably and effectively improve the efficiency of traditional TBB.

### *B. Real CT Image Modeling Simulation*

The preceding discussions primarily rely on binary tree concepts and principles, yet the lung bronchial branching pattern does not adhere to a fixed binary structure [29]. For instance, the left main bronchus divides into upper and lower lobe bronchi, while the right main bronchus splits into upper, middle, and lower lobe bronchi. A bronchiole may further branch into multiple thinner bronchi, with branching number and direction influenced by lung tissue structure and function. To ensure the planning theory applies to real bronchial models, this research uses binary tree logic to define feature points and branches during bronchial centerline extraction. When an actual bronchial bifurcation point has more than two branches, it is automatically decomposed into multiple binary bifurcation points to ensure the binary tree structure. The process effectively restore the appearance of the bronchial centerline, verifying the binary tree approach's feasibility and scientific validity.

TABLE I

THE FINAL PLANNED MULTI-SAMPLE TBB PATH

| Bronchial Area | Start Point (Bifurcation) | End Point (Bifurcation) | Number of Passes |
|---|---|---|---|
| Main | (-0.71, -7.06, -63.53) | (-2.06, 11.71, -136.17) | 5 |
| Left | (-2.06, 11.71, -136.17) | (-16.02, 15.29, -151.06) | 3 |
| | (-16.02, 15.29, -151.06) | (-28.30, 13.17, -177.65) | 2 |
| | (-28.30, 13.17, -177.65) | (-32.18, 15.17, -183.56) | 2 |
| | (-32.18, 15.17, -183.56) | (-38.16, 14.40, -198.47) | 2 |
| | (-38.16, 14.40, -198.47) | (-43.00, 10.55, -202.49) | 1 |
| | (-43.00, 10.55, -202.49) | (-47.53, 5.10, -212.86) | 1 |
| | (-16.02, 15.29, -151.06) | (-31.93, 14.18, -146.55) | 1 |
| | (-38.16, 14.40, -198.47) | (-41.11, 17.02, -206.07) | 1 |
| | (-41.11, 17.02, -206.07) | (-41.96, 21.87, -213.15) | 1 |
| | (-41.96, 21.87, -213.15) | (-43.41, 24.60, -220.83) | 1 |
| Right | (-2.06, 11.71, -136.17) | (35.53, 17.30, -163.87) | 2 |
| | (35.53, 17.30, -163.87) | (41.99, 20.65, -174.46) | 1 |
| | (41.99, 20.65, -174.46) | (53.80, 20.25, -194.51) | 1 |
| | (53.80, 20.25, -194.51) | (53.94, 20.65, -195.59) | 1 |
| | (53.94, 20.65, -195.59) | (60.54, 22.07, -207.30) | 1 |
| **Z = 839.29** | | | |

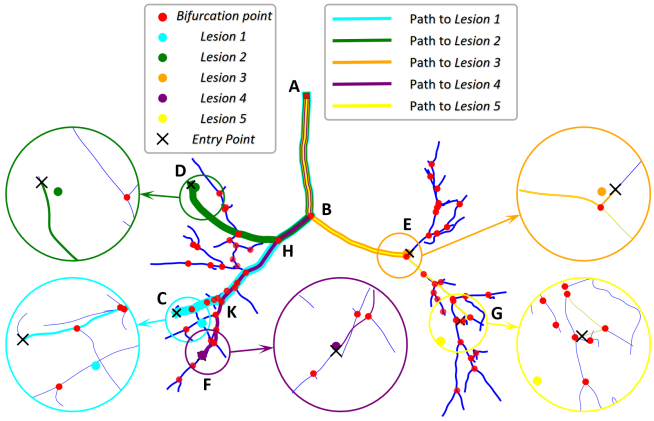


Fig. 9. Multi-sample TBB path for five lesions.

Building on the aforementioned foundation, Mimics (Mimics 21.0, Materialise NV, Leuven, Belgium) was applied for 3D reconstruction and 3D Slicer (Version 5.8.1) was used to do centerline extraction in this research. Operational details are illustrated in Fig. 8.

To scientifically validate the proposed method's feasibility in real TBB operations, a set of CT sequence images from the open-source Cancer Moonshot Biobank - Lung Cancer Collection (CMB-LCA) dataset [29] was utilized for bronchial 3D reconstruction. The centerline obtained in Fig. 8 is used to simulate the planning of multi-target biopsy using the proposed method, and DFS path planning is performed for $P_1$, $P_2$, and $P_3$ obtained for each lesion awaiting biopsy. For this bronchial model, 5 lesions were randomly specified, and according to the principle of minimum resistance, the final planned multi-sample path can be referred to Table I, which includes the coordinates of the starting and ending bifurcation points of each bronchus in the biopsy path, as well as the number of times the bronchoscopic robot passes through this segment of bronchus in the case of multi-inspection at one time (the rightmost column).

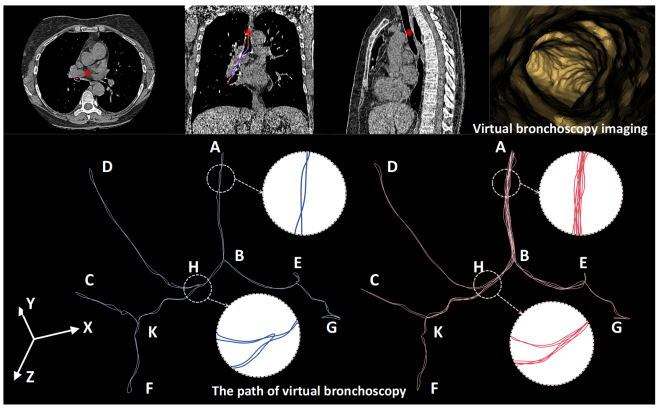


Fig. 10. Comparison of simulated bronchoscope paths for the proposed multi-sample and the one-sample TBB method.

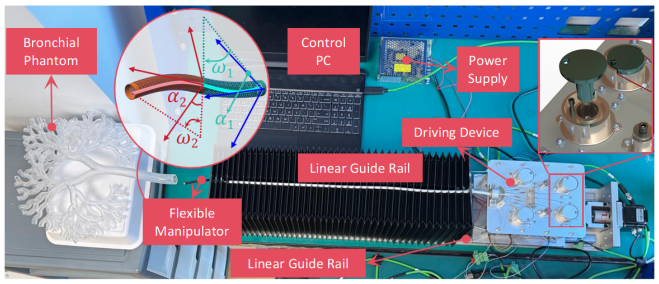


Fig. 11. Bronchoscopic robotic prototype and bronchial phantom.

According to the path data in Table I, a multi-sample TBB visualization path for the five lesions of the bronchial model can be drawn as Fig. 9.

To validate that the proposed method effectively reduces TBB consuming time, a virtual bronchoscopy simulation was conducted on the bronchial model, as shown in Fig. 10. The blue line depicts the optimized path using the proposed strategy, while the red line represents the traditional one-sample TBB trajectory. Bifurcation points labeled with letters correspond to those in Fig. 9. Results demonstrate that compared to unoptimized multi-target detection, the multi-sample TBB path optimization strategy shortens total movement distance by over 60%, significantly enhancing TBB efficiency.

### C. Experimental Verification

In order to verify that the proposed method can effectively guide TBB path for actual prototype, this Section applies the multi-sample TBB planning strategy to an actual bronchoscopic robot and an 8-level transparent bronchial phantom. The manipulator consists of two continua, each of which is driven by four tendons to control the bending angle $\omega$ and the bending plane angle $\alpha$, as shown in Fig. 11. The two tendons that control the same $\omega$ are controlled by the same turntable, one side is tightened and the other side is relaxed. Each turntable is driven by a micro stepper motor (STM2851B-CANopen-M, NiMotion, China) with its integrated encoder and driver. At the bottom of the drive module is a linear slide that controls the feed and retraction of the manipulator, which is driven by a stepper motor (STM5741A-CANopen-E, NiMotion, China) with its integrated encoder and driver.

First, the scientificity and operability of the equivalent resistance proposed in section II is verified. Assume that 8 different lesions are in the (hypothetical) lung space of the bronchial phantom, and their $P_1$, $P_2$ and $P_3$ and the corresponding paths are shown in Fig. 12.The bronchoscopic robot was used to perform a reaching test for each three points. It shows that for a lesion, the selection of different $P$ has a direct impact on bronchoscopic operation, whose average time of each 10 tests is marked in Fig. 12.

In addition, in order to verify the efficiency of the proposed multi-sample TBB method compared with traditional one-sample TBB method, 3-8 lesions above were randomly selected, and the bronchoscopic robot is used to do the arrival test. The optimal paths corresponding to 8 lesions are shown in the upper left corner of Fig. 12. The time comparison for different number of lesions with the two operations is shown in Fig. 13, which shows that the average consuming time

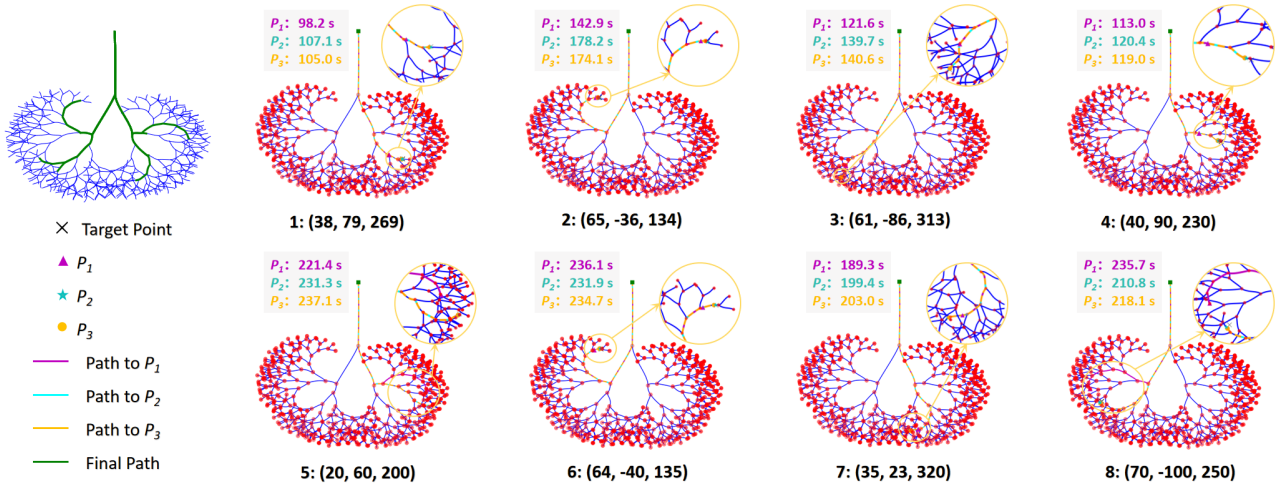


Fig. 12. Lesion distribution in phantom with target points and average operation time.

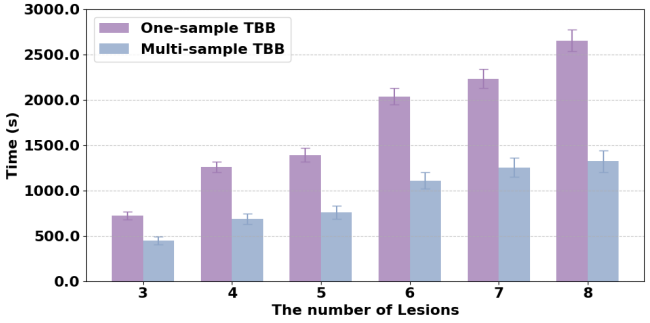


Fig. 13. Comparison of consuming time between one-sample and multi-sample TBB for different number of lesions.

of multi-sample TBB is reduced over 40% compared with traditional one-sampe TBB, greatly improving the efficiency.

## IV. Conclusion

In this paper, a multi-sample TBB planning method was proposed to solve the clinical problem of low diagnostic efficiency of multiple pulmonary nodules in TBB. This research innovatively abstracted the bronchial morphology into resistive circuits, transformed the optimal path planning of multi-sample TBB into equivalent resistance minimization, constructing a new TBB path planning framework. This framework breaks through the limitations of traditional one-sample TBB path optimization, and provides theoretical support for multi-sample TBB operations. Besides, compared with the single shortest path principle in traditional path planning, the proposed method established an evaluation system that comprehensively considers multiple factors such as bronchial morphology and locations of lesions, and replaced the traditional standard with the principle of minimum equivalent resistance.

## References


[1] B. Zhao, L. Zeng, Z. Wu, and K. Xu, "A continuum manipulator for continuously variable stiffness and its stiffness control formulation," *Mech. Mach. Theory*, vol. 149, no. 103746, 2020.

[2] X. Gao, X. Li, C. Zhao, L. Hao, and C. Xiang, "Variable stiffness structural design of a dual-segment continuum with independent stiffness and angular position," *Rob. Comput. Integr. Manuf.*, vol. 67, no. 102000, 2021.

[3] D. Sui, S. Zhao, T. Wang, Y. Liu, Y. Zhu, and J. Zhao, "Design of a bio-inspired extensible continuum manipulator with variable stiffness," *J. Bionic Eng.*, vol. 22, pp. 181–194, 2025.

[4] C. Chautems, A. Tonazzini, Q. Boehler, S. H. Jeong, D. Floreano, and B. J. Nelson, "Magnetic continuum device with variable stiffness for minimally invasive surgery," *Adv. Intell. Syst.*, vol. 2, no. 1900086, 2020.

[5] E. Amanov, T.-D. Nguyen, S. Markmann, F. Imkamp, and J. Burgner-Kahrs, "Toward a flexible variable stiffness endoport for single-site partial nephrectomy," *Ann. Biomed. Eng.*, vol. 46, no. 10, pp. 1498–1510, 2018.

[6] A. Kitamura, K. Okafuji, R. Imai, M. Murakami, S. Ro, Y. Tomishima, T. Jinta, N. Nishimura, and T. Tamura, "Reproducibility of peripheral branches in virtual bronchoscopic navigation using vincent and lung-point software for peripheral lung lesions," *Respiratory Investigation*, vol. 59, no. 6, pp. 772–776, 2021.

[7] W. A. Baaklini, M. A. Reinoso, A. B. Gorin, A. Sharafkaneh, and P. Manian, "Diagnostic yield of fiberoptic bronchoscopy in evaluating solitary pulmonary nodules," *Chest*, vol. 117, no. 4, pp. 1049–1054, 2000.

[8] B. L. Conrad, J. Jung, R. S. Penning, and M. R. Zinn, "Interleaved continuum-rigid manipulation: An augmented approach for robotic minimally-invasive flexible catheter-based procedures," in *Proc. IEEE Int. Conf. Robot. Autom. (ICRA)*, pp. 718–724, 2013.

[9] W. Zhao, J. Wang, and Y. Fei, "A multigait continuous flexible snake robot for locomotion in complex terrain," *IEEE/ASME Trans. Mechatron.*, vol. 27, no. 5, pp. 3751–3761, 2022.

[10] T. Lim, P. Cheang, and F. Scarpa, "Wave motion in auxetic solids," *Phys. Status. Solidi. (b)*, vol. 251, no. 2, 2014.

[11] K. T. Chan, K. F. Lai, N. G. Stephen, and K. Young, "A new method to determine the shear coefficient of timoshenko beam theory," *J. Sound. Vib.*, no. 14, pp. 3488–3497, 2011.

[12] R. Kupferman and J. P. Solomon, "A riemannian approach to reduced plate, shell, and rod theories," *J. Funct. Anal.*, vol. 266, no. 5, pp. 2989–3039, 2014.

[13] S. Kordkheili, H. Bahai, and M. Mirtaheri, "An updated lagrangian finite element formulation for large displacement dynamic analysis of three-dimensional flexible riser structures," *Ocean Eng.*, vol. 38, no. 5-6, pp. 793–803, 2011.

[14] C. Wang, C. G. Frazelle, J. R. Wagner, and I. D. Walker, "Dynamic control of multisection three-dimensional continuum manipulators based on virtual discrete-jointed robot models," *IEEE/ASME Trans. Mechatron.*, vol. 26, no. 2, pp. 777–788, 2021.

[15] H. S. Hedia, S. Aldousari, and N. Fouda, *Theory of Elasticity and Plasticity*. King Abdulaziz University, 2017.

[16] H. Wang, C. Wang, W. Chen, X. Liang, and Y. Liu, "Three-dimensional dynamics for cable-driven soft manipulator," *IEEE/ASME Trans. Mechatron.*, vol. 22, no. 1, pp. 18–28, 2017.

[17] E. Harsono, J. Yang, S. Bhattacharya, and H. Yu, "Design and analysis of a novel hybrid-driven continuum robot with variable stiffness," *Mech. Mach. Theory*, vol. 177, p. 105067, 2022.

[18] G. Qin, H. Wu, and A. Ji, "Equivalent dynamic analysis of a cable-driven snake arm maintainer," *Front. Robot. AI*, vol. 12, no. 15, p. 7494, 2022.

[19] Y. Kong, S. Song, N. Zhang, J. Wang, and B. Li, "Design and kinematic modeling of in-situ torsionally-steerable flexible surgical robots," *IEEE Robot. Autom. Let.*, vol. 7, no. 2, pp. 1864–1871, 2022.

[20] W. Hong, F. Feng, L. Xie, and G. Yang, "A two-segment continuum robot with piecewise stiffness for maxillary sinus surgery and its decoupling method," *IEEE/ASME Trans. Mechatron.*, vol. 27, no. 6, pp. 4440–4450, 2022.

[21] D. G. Spampinato, U. Sridhar, and T. M. Low, "Linear algebraic depth-first search," in *Proceedings of the 6th ACM SIGPLAN International Workshop on Libraries, Languages and Compilers for Array Programming*, ARRAY 2019, (New York, USA), p. 93–104, Association for Computing Machinery, 2019.

[22] L. Huang, B. Liu, L. Yin, P. Zeng, and Y. Yang, "Design and validation of a novel cable-driven hyper-redundant robot based on decoupled joints," *J. Robot.*, vol. 2021, 2021.

[23] A. Tariverdi, V. K. Venkiteswaran, M. Richter, O. J. Elle, J. Trresen, K. Mathiassen, S. Misra, and R. G. Martinsen, "A recurrent neural-network-based real-time dynamic model for soft continuum manipulators," *Front. Robot. AI*, vol. 8, p. 631303, 2021.

[24] Z. Wu, Q. Li, J. Zhao, J. Gao, and K. Xu, "Design of a modular continuum-articulated laparoscopic robotic tool with decoupled kinematics," *IEEE Robot. Autom. Let.*, vol. 4, no. 4, pp. 3545–3552, 2019.

[25] K. Cheng, L. Li, Y. Du, J. Wang, Z. Chen, J. Liu, X. Zhang, L. Dong, Y. Shen, and Z. Yang, "A systematic review of image-guided, surgical robot-assisted percutaneous puncture: Challenges and benefits.," *Math. Biosci. Eng.*, vol. 20 5, pp. 8375–8399, 2023.

[26] M. Baumhauer, T. Simpfendörfer, B. P. Müller-Stich, D. Teber, C. N. Gutt, J. Rassweiler, H. P. Meinzer, and I. Wolf, "Soft tissue navigation for laparoscopic partial nephrectomy," *Int. J. Comput. Ass. Rad.*, vol. 3, pp. 307–314, 2008.

[27] D. Hill, T. Williamson, C. Y. Lai, M. Leary, and M. Brandt, "Robots and tools for remodeling bone," *IEEE Reviews in Biomed. Eng.*, vol. 13, pp. 184–198, 2020.

[28] L. A. Saiz, H. C. Groen, W. J. Heerink, and T. J. M. Ruers, "The influence of the da vinci surgical robot on electromagnetic tracking in a clinical environment," *J. Robot Surg.*, vol. 18, pp. 18–54, 2024.

[29] Cancer-Moonshot Biobank, *Cancer Moonshot Biobank - Lung Cancer Collection (CMB-LCA)*. The Cancer Imaging Archive, 2022.